UCRL--96665

DE88 000224

AXIAL POWER LOSS ALONG OPEN FIELD LINES

Donald L. Correll

This paper was prepared for submittal to the
Course/Workshop on Physics of Mirrors,
Reversed Field Pinches and Compact Tori,
Varenna, Italy
September 1-11, 1987

August 1, 1987

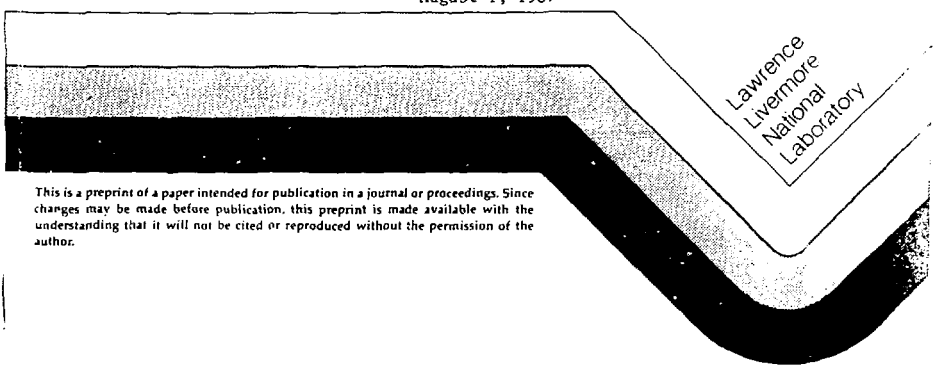

Axial Power Loss Along Open Field Lines*

Donald L. Correll
Lawrence Livermore National Laboratory, University of California
Livermore, CA 94550 U.S.A.

ABSTRACT

Studies are underway to evaluate the linear mirror geometry as a candidate for a high-fluence, neutron irradiation facility. This steady-state, low-Q design is currently perceived to comprise a two-component plasma driven by neutral beams with mirror confinement of the hot ions and with no electrostatic axial reduction in the warm ion end losses. Warm-ion fueling and end-wall power density will require substantial cold plasma exterior to the mirror cell and neutral gas near the end wall. In this paper, we evaluate to what extent the loss power parallel to the axial magnetic field along open field lines is a function of the escaping plasma and end-wall parameters. By allowing the source power to depend directly on the plasma density and electron temperature, several new conclusions may be pertinent to closed field-line geometries with open field-line divertors.

*This work was performed under the auspices of the U.S. Department of Energy by Lawrence Livermore Laboratory under contract No. W-7405-ENG-48.

I. INTRODUCTION

Mirror-type plasmas with two distinct ion components were first modeled by R.F. Post et al.[1] as fusion reactor candidates with

$$Q \equiv \frac{\text{nuclear power out}}{\text{neutral beam power in}} \approx 1. \tag{1}$$

The two ion components consisted of a high-energy deuterium component, injected from neutral-beam sources ($\approx$ 200 kV), and a low-temperature tritium plasma target. With the $Q \gg 1$ concept definition of electrostatic plus magnetic confinement geometries in conventional tandem mirrors[2,3] followed by thermal-barrier tandem mirrors,[4] the two-component, large-mirror-ratio ($R \approx 10$), single-cell geometry was set aside.

Recently, a renewed interest in the single-cell mirror has been driven by design studies[5] for a steady-state, low Q plasma neutron source. To reduce the technology and physics requirements, present designs use the minimum mirror ratio and radial well-depth for micro- and macrostability requirements of the hot ions as well as electrostatic axial reduction in the end losses of the warm ions.[5] This paper summarizes the axial power flow in such a plasma neutron-source device at high density ($n \approx 10^{15}\ cm^{-3}$) and at low electron temperature ($T_e \approx 100\ eV$). An axial power flow review is necessary because fueling requirements of the warm ion component and power density considerations at the end wall will require substantial cold plasma and neutral gas at the axial boundaries of the plasma. These review calculations may also be relevant to the Gas Dynamic Trap[6] concept, which employs collisional plasma densities external to the mirror cell for MHD stabilization.

Proposed operation at high enough densities and at low enough temperatures to demand that electron collisionality be considered in power balance is somewhat novel to past fusion-relevant mirror studies. However, design work on reactor-size tokamaks–for example, INTOR[7]–has shown that low-temperature, collisional plasmas could solve the problem of handling large heat fluxes (tens of megawatts) on divertor plates.[8] Many of the ideas and equations for this paper were stimulated by Refs. 9 and 10.

R.F. Post[11] reviewed the earlier work of Hobbs and Wesson[12] and Morse[13] on thermal transport, including collisional effects, in machines with open magnetic field lines. However, Ref. 12 only considers uniformly distributed heating of electrons, and Ref. 13 forces the electron temperature to be zero at the end wall. The present paper adds the appropriate equations and boundary conditions to relax these two constraints. Sec. II summarizes the power flow in classical, one ion-component plasmas in mirrors, and Sec. III describes two-component thermal heat flow from hot ions to electrons to warm ions with axial power loss dominated by thermal conductivity or convection along a plasma column with open field lines that terminates in either a solid or a gas end-wall condition.[14] Section IV applies the model of Sec. III to a specific case for illustration and discussion.

II. REVIEW OF A CLASSICAL, ONE ION-COMPONENT MIRROR

This review of the classical, one ion-component mirror defines the various time scales pertinent to the two ion-component discussion of Sec. III.

Open magnetic field lines in a mirror device allow particles to escape axially by pitch angle diffusion in velocity space in addition to radial spatial diffusion as in closed field-line geometries. In a classical mirror machine with mirror ratio, R, there exists a single ion component with an energy, E_{hot}, and a density, $n_{hot} = n_e$, with n_e equal to the electron

density. Because the electron tempertaure, T_e, is always less than E_{hot} and the ion mass, $M \gg m_e$ (the electron mass), the electrons pitch angle scatter much faster than the ions. A positive electrostatic potential, ϕ_0, develops with respect to the end wall to augment the electron confinement, which allows the ion (magnetic only) and electron (magnetic plus electrostatic) axial particle losses to remain equal. Mathematically, this result is given by:[15]

$$\tau_{ii} \approx \tau_{ee} G(R) \frac{e\phi_0}{T_e} exp(\frac{e\phi_0}{T_e}), \tag{2}$$

where the ion-ion 90°, self-scattering time is

$$\tau_{ii} = \frac{2.5 \times 10^{11} E_{hot}^{3/2}(keV) M^{1/2}(amu)}{n_{hot} ln\Lambda}; \tag{3}$$

the electron self-scattering time is

$$\tau_{ee} = \frac{1.1 \times 10^{10} T_e^{3/2}(keV)}{n_e ln\Lambda}; \tag{4}$$

and the coulomb logarithm

$$ln\Lambda \propto ln \frac{T_e^{3/2}}{n_e} \tag{5}$$

varies slowly from a value of 10 at 10 eV and 10^{15} cm^{-3} to a value of 20 at 10 keV and 10^{12} cm^{-3}. The units for ion or electron plasma density are cm^{-3} in every equation in this paper. The term $G(R)$ is a weak function of the mirror ratio, R, and has a nominal value of three for practical values of R from 2 to 20. Equation (2) predicts values of ϕ_0/T_e which range from three to seven.

Energy exchange between the hot ions and electrons is given by the electron "drag" time necessary for an ion to have its energy lowered by one e-folding through collisions with thermal electrons:

$$\tau_d = \frac{1.0 \times 10^{13} M T_e^{3/2}(keV)}{n_e ln\Lambda}. \tag{6}$$

For deuterium ions ($M = 2$), Eqs. (3) and (6) imply that

$$\tau_d (for\ T_e < \frac{E_{hot}}{15}) < \tau_{ii}. \tag{7}$$

Under the circumstances of Eq. (7), the main channel for axial power loss is through the electron end losses. When the plasma density external to the mirror cell is low enough that thermal conduction can be ignored (the opposite case is treated in detail in Sec. III on two ion-component plasmas), the minimum electron power loss is described by

$$\frac{n_{hot} E_{hot} L_{hot}}{\tau_d} = 2J_{loss}^{ion}(\phi_0 + T_e) + 2J_{secondary} T_e, \tag{8}$$

where L_{hot} is the hot ion length; J_{loss}^{ion} is the current density of axial ion end losses per end; and

$$J_{loss}^{ion} = J_{loss}^{electron} - J_{secondary} \tag{9}$$

allows for a secondary electron-emission current at the end wall. It is quite common to represent $J_{secondary}$ as

$$J_{secondary} = \frac{\lambda}{1-\lambda} J_{loss}^{ion} = \lambda J_{loss}^{electron}, \tag{10}$$

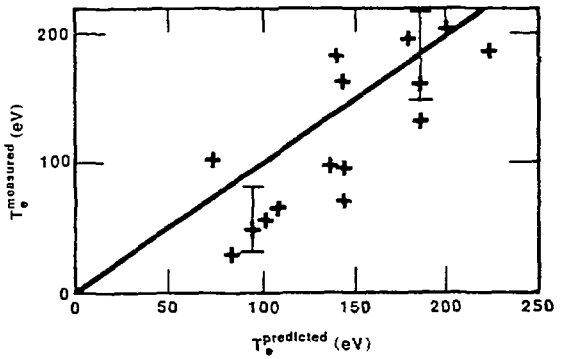

Figure 1: The measured electron temperature from TMX-U data vs the predicted value from Eq. (11).

where λ is the secondary emission coefficient and varies for a cold, solid end wall from 0.4 to 0.9, depending on plasma parameters and end-wall conditions.[16] The magnitude of J_{loss}^{ion} can vary from the minimum value set by the classical axial particle losses of the hot ions to many times this value due to marginal stability requirements of "loss-cone" velocity distribution instabilities.[17,18]

Combining Eqs. (8) and (10) with $\tau_d \equiv k_d \frac{T_e^{3/2}}{n_e}$ results in the familiar 5/2 scaling law for T_e:

$$T_e^{5/2} = \left[\frac{n_e n_{hot} E_{hot} L_{hot}}{2 k_d J_{loss}^{ion}}\right]\left[\frac{1}{\frac{\phi_0}{T_e} + \frac{1}{1-\lambda}}\right]. \qquad (11)$$

Perhaps the best example of the 5/2 scaling law for T_e is given by a set of data from TMX-U operation without thermal barriers shown in Fig. 1.[19] The measured on-axis central-cell electron temperature data points are plotted against the predicted values from Eq. (11) using concurrent data for all input parameters and setting λ equal to zero. The solid line indicates perfect agreement between measured and predicted values. A reasonable assumption of $\lambda = 0.7$ reduces the predicted value for T_e by 18% for these data with $\frac{\phi_0}{T_e} \approx 5$. The agreement in Fig. 1 is good enough to conclude that electron axial power loss for this data set is essentially classical because Eq. (11) predicts the measured values.

The next section addresses electron axial power losses when two ion components are present, and the warm component is at sufficiently high enough density to require collisional power losses to be considered.

III. TWO ION-COMPONENT AXIAL POWER FLOW

In this section, a set of analytical equations is used to describe the axial power flow in a two ion-component plasma.[20] Power flows from mirror-confined hot ions to thermal

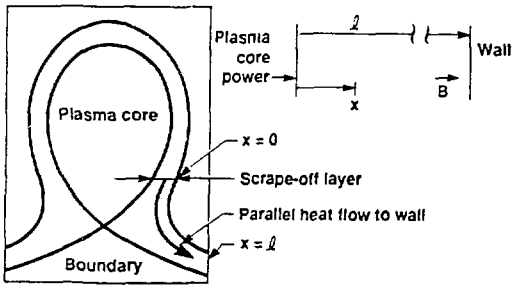

Figure 2: Schematic of the geometry used in Ref. (21) for boundary heat flow in a divertor.

electrons, which in turn heat a warm ion component. The electron density is high enough to require that both conduction and convection axial power losses be considered.

The following discussion follows closely the work by Mahdavi et al. on power losses along open field lines in the divertor of the D-III tokamak.[21] There is, however, one major difference. Ref. 21 looks at various limits to the axial power losses for different values of n_e without considering the dependence of the power input on plasma density and electron temperature; the following analysis allows for a direct dependence on n_e and T_e through the ion-electron drag time given in Eq. (6). The geometry of Ref. 21 is given by Fig. 2, which can be compared to the geometry presently under discussion in this paper (Fig. 3). Figure 3 defines schematically the geometry in terms of three regions.

Region 1 represents the volume, $V_1 = 2L_1A_1$, containing a population of mirror-confined, hot ions of energy, E_{hot}, and of density, n_{hot}, with a dominant power loss at $T_e < \frac{E_{hot}}{15}$ given by energy exchange with the electron population at a rate

$$P_1(W) = \frac{qn_{hot}(cm^{-3})E_{hot}(eV)V_1(cm^3)}{\frac{k_d T_{e1}^{3/2}(eV)}{n_{e1}(cm^{-3})}}, \tag{12}$$

where $q = 1.6 \times 10^{-19}\ J/eV$ and $k_d = 6 \times 10^7\ s \cdot cm^{-3} \cdot eV^{-3/2}$ for $ln\Lambda \approx 10$ with deuterium ($M = 2$) hot ions (see Eqs. 5 through 7). The subscript 1 refers to parameter values within Region 1. Also present in this region is a population of warm ions of density, n_{warm1}, which transits all three regions, as do the electrons, and which satisfies

$$n_{e1} = n_{hot} + n_{warm1}. \tag{13}$$

Because the energy exchange time between the hot and warm ions is approximately τ_{ii} (see Eq. (3)), there is no appreciable power loss due to ion-ion collisions. The Subscript 1 has been dropped from n_{hot} because the hot ions are modeled as having a finite density only in Region 1. Therefore, at all points in z outside of Region 1, the following is assumed:

$$n_e = n_{warm}, \tag{14}$$

unless the conditions in Region 3 demand that a population of cold ions, n_{cold}, be included in the modeling. Strictly speaking, the hot ions and electrons could have different lengths

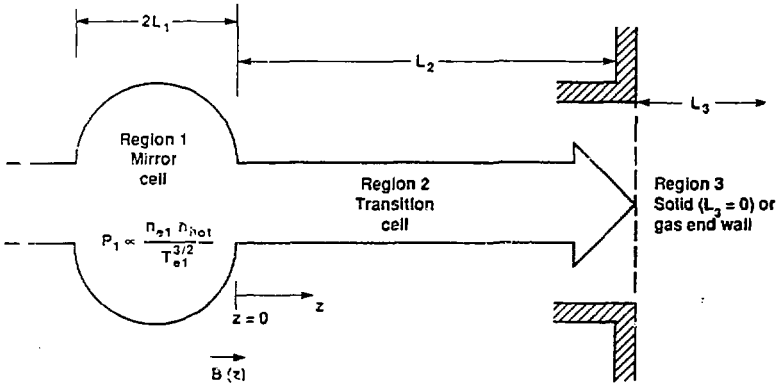

Figure 3: Schematic of the geometry under discussion for axial power loss along open field lines.

in Region 1, but this additional complexity to the equation can be ignored without any changes in the desired conclusions.

Region 2 represents a collisionally dominated plasma column where the electron-electron mean free path, $\lambda_{ee} = v_e \tau_{ee}$, can be expressed as

$$\lambda_{ee} = \frac{2 \times 10^{13} T_e^2(eV)}{n_e ln\Lambda}, \tag{15}$$

and is small compared to the column length ($\lambda_{ee} < L$). Under these circumstances, the power flow is described by the thermal conductivity expression[22] derived by Spitzer

$$P_2(W) = -k_{tc} T_{e2}^{5/2}(eV) \frac{dT_{e2}(z)}{dz} A_2(cm^2) \tag{16}$$

where $k_{tc} = \frac{3.1 \times 10^2}{ln\Lambda}\ W \cdot eV^{-7/2} \cdot cm^{-1}$. For reference, if $\lambda_{ee} > L$, then collisionless power flow due to thermal convection, as described in Eq. (8), is the proper expression to use. Under these conditions, the Pastukhov[15] potential, ϕ_0, lowers the electron particle flux, which ensures that the electron heat flux remains below the upper bound given by $n_e v_e T_e$.

For this paper's one-dimensional discussion of axial power flow, both radiation and radial transport losses are ignored. The heat loss from the electron population in Region 2 due to warm ion-electron energy equipartition is included by adding the ion-convection losses to the electron-convection losses set by the end-wall boundary condition in Region 3. The ion-conduction term is not included because the thermal conduction coefficient, $K - tc$, for ions is $(m_e/M)^{\frac{1}{2}}$ times smaller than the electron value. Thermal losses associated with axial gradients in potential or density are assumed to be small compared to that associated with the electron temperature gradient.

Region 3 represents the power flow limit of the total energy carried to the axial boundary by an ion, electron pair. This end-wall boundary condition[12,23] can be written as:

$$P_3(W) = n_{e3}(cm^{-3})qc_s(cm/s)A_3(cm^2)\cdot \left[2T_{warm3}(eV) + 2T_{e3}(eV) + \frac{\lambda}{1-\lambda}T_{e3}(eV) - \phi_{sheath}(eV)\right] \quad (17)$$

where $q = 1.6 \times 10^{-19}$ C. T_{warm} is the warm ion temperature, and $c_s = \left(\frac{T_{warm3} + T_{e3}}{M_{warm}}\right)^{1/2}$ is the acoustic speed. The product nqc_s plays the same role in Eq. (17) as J_{loss}^{ion} does in Eq. (8). The sheath potential, ϕ_{sheath}, can be related to the secondary electron-emission coefficient, λ, defined in Eq. (10), according to Hobbs and Wesson,[12] through

$$q\phi_{sheath} = T_{e3}ln\left[\left(\frac{M_{warm}}{2\pi m_e}\right)^{1/2}(1-\lambda)\right], \quad (18)$$

where $0 < \lambda < 1 - 8.3\left(\frac{m_e}{M_{warm}}\right)^{1/2} \approx 0.9$ for tritium is the upper bound value set by an electron emitting wall with a double sheath.[12] The Hobbs and Wesson expression for P_3 is proportional to v_e, not c_s; therefore, according to their convention, $P_3 = \frac{1}{4}n_e v_e 2T_e F$. The term $F(\lambda)$ without sheath effects is one and, with sheath effects, varies from 0.12 (no secondaries, $\lambda = 0$) to 0.37 (double sheath, $\lambda = 0.9$). This paper uses Eq. (17) because it resembles more closely previous mirror power flow papers.[16,17,20]

Because the only power source in this problem is in Region 1, then as suggested in Ref. 21, the following is true:

$$\frac{1}{2}P_1 = P_2 = P_3, \quad (19)$$

where the factor 1/2 allows for the input power to flow symmetrically to each end wall. If n_e is large enough to assume $T_e = T_{warm}$ at all z then Eq. (17) can be rewritten as

$$P_3(W) = n_{e3}qA_3k_aT_{e3}^{1/2}(\gamma+4)T_{e3} \quad (20)$$

where the acoustic speed, $c_s = (\frac{m_e}{M_{warm}})^{1/2}v_e \equiv k_aT_e^{1/2}(eV)$ with $k_a = 8 \times 10^5$ $cm/s \cdot eV^{-1/2}$ for tritons, and $\gamma \equiv q\frac{\phi_{sheath}}{T_e} + \frac{\lambda}{1-\lambda}$. For reference, the electron thermal velocity, $v_e\ (cm/s) = \left(\frac{2T_e}{m_e}\right)^{\frac{1}{2}} = 6 \times 10^7\ T_e^{\frac{1}{2}}(eV)$.

The integral solution to $\frac{1}{2}P_1 = P_2$ gives

$$\frac{\frac{7}{2}z}{k_{ic}A_2}\left[\frac{qn_{hot}E_{hot}L_1A_1n_{e1}}{k_dT_{e1}^{3/2}}\right] = T_{e1}^{7/2} - T_{e2}^{7/2}(z), \quad (21)$$

where the units are defined in Eqs. (12) and (16) and where the ion-electron drag expression in brackets on the LHS has a direct dependence on both n_e and T_e in contrast to the input power term in Eq. (4) of Ref. 21.

Rearranging the results from solving $\frac{1}{2}P_1 = P_3$ with the axial pressure balance assumption, $n_{e1}T_{e1} = n_{e3}T_{e3}$, gives an expression for the end-wall T_e in terms of the midplane value of T_e:

$$T_{e3}^{1/2} = T_{e1}^{-5/2}\frac{n_{hot}E_{hot}L_1A_1}{k_ak_dA_3(\gamma+4)}. \quad (22)$$

Equation (22) can be substituted into Eq. (21), and the result evaluated at $z = L_2$ with $T_{e2}(L_2) \equiv T_{e3}$ to produce an expression for T_{e1}:

$$T_{e1}^{21} = \left[\frac{7}{2} L_2 \frac{q n_{hot} E_{hot} L_1 A_1 n_{e1}}{k_e k_d A_2}\right] T_{e1}^{16} - \left[\frac{n_{hot} E_{hot} L_1 A_1}{k_e k_d A_2 (\gamma + 4)}\right]^7. \tag{23}$$

The immediate response to an equation such as Eq. (23) is that nothing physical can depend on the electron temperature to the 21st power! However, except for minor changes in definitions of lengths and the acoustic speed, Eq. (23) is exactly the result one would obtain from Eq. (5) of Ref. 21 if the input power term were replaced by the ion-electron drag expression, Eq. (12), with a $n_e T_e^{-3/2}$ dependence.[24]

By examining the limits where either one or the other term on the RHS of Eq. (23) dominates, one can further explain the sensitivity to the magnitude of T_{e1}. In the extreme conduction (large n_{e1}) limit to the power flow where T_{e3} is commonly assumed to be near zero, the T_{e1} solution to Eq. (21) with $T_{e2}(L_2) = T_{e3} = 0$ is the same as one would derive from Eq. (23) by ignoring the second term of the RHS of Eq. (23). The result is

$$T_{e1}^5 = B_{cond}, \tag{24}$$

where Eq. (23) has been rewritten as

$$T_{e1}^{21} = B_{cond} T_{e1}^{16} + C_{conv}^7. \tag{25}$$

In the extreme convection (low n_{e1}) limit to the power flow where dT_e/dz is near zero, the solution to Eq. (22) with $T_{e3} = T_{e1}$ is the same as one would derive from Eq. (23) by ignoring the first term of the RHS of Eq. (23). The result is

$$T_{e1}^3 = C_{conv}. \tag{26}$$

This result has one more 1/2 power for T_e than the 5/2 scaling law of Eq. (11) because J_{loss}^{ion} has been replaced by $n_e q c_s$ with $c_s \propto T_e^{1/2}$.

Therefore, Eq. (23) can be considered the complete solution to axial power flow dominated by electron losses in open-field lines with an input power dependent upon the electron temperature. The limits of the RHS terms of Eq. (23) represent the cases of thermal conduction or convection dominance. Assume for now that the product of the hot ion parameters, n_{hot}, E_{hot}, L_1, and A_1 is constant, i.e., the total energy stored in the hot ions does not change. If Eq. (24) describes the proper limit to Eq. (23)–that is the conduction limit–then T_{e1} depends on $(L_2 n_{e1}/A_2)^{1/5}$. If Eq. (26) describes the proper approximation to Eq. (23)–that is the convection limit–then T_{e1} depends on $[A_3(\gamma + 4)]^{1/3}$.

Section IV evaluates the electron temperature for a mirror plasma neutron source where actual values for the plasma parameters are substituted into Eq. (23).

IV. ELECTRON TEMPERATURE FOR A MIRROR PLASMA NEUTRON SOURCE

Preliminary designs[5] exist to evaluate a plasma neutron source as described in Sec. I. The present concept of a high-intensity (5–10 MW/m^2), high-fluence D-T neutron source consists of a linear, two-component plasma[1] in which injected energetic deuterons react with a warm tritium target. High-energy neutral beams ($E_{injection} \approx 200\ kV$) of deuterium atoms are ionized in the warm, dense tritium target plasma, and the deuterons are trapped

in a quadrupole-mirror field. As the deuterons slow down by coulomb ions with the target electrons, they interact with the tritium to generate the desired D-T fusion neutron flux. Since the drag loss on the electrons is rapid compared to ion-scattering processes, only a low mirror ratio is required to confine the hot ions. The deuterons degrade in energy to the point where nuclear interaction becomes improbable, and they continue to cool until they join the warm target population and diffuse out the ends of the device. The heated electrons share their energy by frequent collisions with target ions, so $T_{iwarm} \approx T_e$ in the warm plasma. Beyond each end of the quadrupole, a transition region comprised of a solenoidal field guides the warm plasma column to the end regions.

The desired neutron flux of 5-10 MW/m^2 is achieved at minimum beam power $\leq$ 50 MW by adjusting the many parameters of the device to an optimum combination that is consistent with technological and physics constraints. One of those constraints is the axial electron temperature profile. The end-wall boundary conditions play a dominant role in determining the electron power balance. A solid end wall is questionable for a steady-state device because of the heat load and sputtering effects [10]. A gas end wall [14] is a possible solution to these two difficulties, but the additional power drain associated with ionization, radiation, and charge-exchange losses due to plasma-neutral atom interactions in the end region can lower the effective end wall T_e. Therefore, electron thermal conduction, as well as convection, has been modeled (Eq. (23) of Sec. III) to evaluate the axial electron temperature. The effect of having a solid versus gas end wall can be bounded, in a simplistic sense, by allowing λ to equal zero for an ideal solid end wall and by setting λ equal to the worst-case value for an electron-emitting end wall,[12] $\lambda = 0.9$, as a pessimistic value for a gas end wall. The value of γ varies from 3.5 to 10 for λ variations from 0 to 0.9, respectively.

The geometry (see Fig. 3) and the plasma parameter design values for the plasma neutron source concept are summarized in Table 1. When evaluated with the values from Table 1, Eq. (23) becomes

$$T_{e1}^{2.1} = \left[1.1 \times 10^5 \frac{L_2 B_2}{B_1}\right] T_{e1}^{1.6} + \left[\frac{2.2 \times 10^7}{\gamma + 4}\right]^7 . \tag{27}$$

where A_1/A_2 in Eq. (23) has been replaced with the ratio of magnetic field strength in Regions 1 and 2 using magnetic flux conservation. The thermal convection limit (see Eqs. 25 and 26) of Eq. (27) gives $T_{e1}^{convection} = 140\ eV$ for an ideal end wall with $\gamma = 3.5$. For the worst-case $\gamma = 10$ (used to approximate any deleterious effects from a gas end wall), $T_{e1}^{convection} = 100\ eV$. In order for the thermal conduction limit (see Eqs. 24 and 25) of Eq. (27) to give $T_{e1} \geq 140\ eV$ the column length, L_2, must be greater than 170 cm. Worth checking is the fact that at $n_e = 10^{15} cm^{-3}$, $T_e = 140\ eV$, and $L_2 = 170\ cm$, $L_2/\lambda_{ee} > 4$, which satisfies the Spitzer thermal conductivity requirement, $\lambda_{ee} < L$.

Due to end-wall power loading concerns, as well as fueling for the warm ions, the end wall for the plasma neutron source of Table 1 is envisioned to be a "gas exhaust" chamber similar to that described in Ref. (14). The associated lower effective end-wall T_e requires a column length, L_2, long enough to allow Spitzer thermal conductivity to isolate Regions 1 and 3. Under these conditions, one can calculate the dependence of the hot-ion power losses, P_1, by substituting the conduction limit of Eq. (27) into Eq. (12). The result of this substitution is

$$P_1^{conduction}(W) = 3.7 \times 10^8 \left[\frac{B_1}{B_2 L_2}\right]^{3/10} . \tag{28}$$

Hence, a longer column length L_2 and a higher magnetic field B_2 in Region 2, compared to Region 1, would lower the required neutral beam power.

Table . Preliminary Design Values for a Mirror Plasma Neutron Source

Region 1 ($B_1 = 4\ T$)	Value
Hot ion length, $2L_1$	30 cm
Hot ion radius, r_1	4 cm
Cross-sectional area, A_1	50 cm^2
Hot ion mass, M_{hot}	2 amu (D^+)
Warm ion mass, M_{warm}	3 amu (T^+)
Total electron density, n_{e1}	$1 \times 10^{15} cm^{-3}$
Hot ion density, n_{hot}	$0.4 \times 10^{15} cm^{-3}$
Warm ion density, n_{warm1}	$0.6 \times 10^{15} cm^{-3}$
Hot ion energy, $E_{hot} = E_{\parallel} (E_{\parallel} \ll E_{\perp})$	60 keV
Warm ion temperature, T_{warm1}	T_{e1}
Electron temperature, T_{e1}	determined in Sec. IV
Region 2 ($B_2 = 12\ T$)	Value
Transition length, L_2	determined in Sec. IV
Cross-sectional area, $A_2 = \frac{B_1 A}{B_2}$	17 cm^2
Region 3	Value
Plasma sheath potential	3.5 (solid wall)
Cross-sectional area, $A_3 \equiv A_2$	17 cm^2
Regions 1, 2, and 3	Value
Coulomb logarithm, $ln\Lambda$	10

Equation (28) with TABLE 1 values of $B_1 = 4\ T$ and $B_2 = 12\ T$ (niobium-tin technology) with $L_2 = 170\ cm$ gives $P_1 = 57\ MW$. Extending L_2 from 170 to 500 cm reduces P_1 from 57 to 41 MW, which is below the 50-MW design level target value. For $L_2 = 500\ cm$, the conduction limit for T_{e1} is 175 eV. The longer length, even at $T_{e1} = 175\ eV$, still satisfies $\lambda_{ee} < L_2$.

V. DISCUSSION

Equation 23 describes the dependence of the midplane electron temperature, T_{e1}, upon the escaping plasma parameters (i.e., collisionality) and the end-wall boundary conditions (i.e., secondary electrons). The input power to the electrons is not assumed to be independent of T_e but is allowed to vary according to Eq. (12), which describes energy exchange between the hot ion species and electrons. The large exponent values for T_{e1} in Eq. (23) come about from simultaneously satisfying the extreme limits of thermal transport given by conduction (Eq. 24) and by convection (Eq. 26). When applied to the practical problem of a mirror-based, plasma neutron source (see Sec. IV), Eq. (23) allows the plasma column length to be determined within the limits of available neutral beam power, of magnetic field strength, and of uncertainties in axial boundary conditions.

ACKNOWLEDGMENT

The author wishes to acknowledge valuable discussions with T.A. Casper, D.N. Hill, A.H. Futch, L.L. LoDestro, W.M. Nevins, and T.D. Rognlien.

References

[1]R.F. Post et al., Phys. Rev. Lett. *31*, 280 (1973).

[2]T.K. Fowler and B.G. Logan, Comments, Plasma Phys. Controlled Fusion 2, 167 (1977).

[3]G.I. Dimov et al., Sov. Plasma Phys. *2*, 326 (1976).

[4]D.E. Baldwin and B.G. Fowler, Phys. Rev. Lett. *43*, 1318 (1979).

[5]F.H. Coensgen, Bull. Amer. Phys. Soc., 29th Annual Meeting of APS-DPP (1987). Also see paper by A.H. Futch et al., same meeting.

[6]D.D. Ryutov, Plasma Physics and Controlled Fusion *28*, 191 (1986).

[7]International Tokamak Reactor (INTOR): Zero Phase (IAEA, Vienna, 1980).

[8]M. Petravic et al., Phys. Rev. Lett. *48*, 326 (1982).

[9]C.J. Joachain and D.E. Post, eds., *Atomic and Molecular Physics of Controlled Thermonuclear Fusion*, Plenum Press, New York (1982).

[10]D.E. Post and R. Behrisch, eds., *Physics of Plasma-Wall Interactions in Controlled Fusion*, Plenum Press, New York (1984).

[11]R.F. Post, J. of Nucl. Mater. *76*, 112 (1978).

[12]G. Hobbs and J. Wesson, Plasma Physics *9*, 85 (1967).

[13]R.L. Morse, Physics of Fluids *16*, 545 (1973).

[14]F.R. Chang and J.L. Fisher, Nucl. Fusion *22*, 1003 (1982).

[15]V.P. Pastukhov, Nucl. Fusion *14*, 3 (1974).

[16]G.D. Porter, Nucl. Fusion 22, 1279 (1982).

[17]H.L. Berk et al., Nucl. Fusion *18*, 1379 (1978).

[18]T.A. Casper and G.R. Smith, Phys. Rev. Lett. 48, 1015 (1982).

[19]T.C. Simonen et al., Lawrence Livermore National Laboratory, UCRL-96484 (1987), to be published in IEEE Trans. on Plasma Science.

[20]T.D. Rognlien and T.A. Brengle, Physics of Fluids *24*, 871 (1981).

[21]M.A. Mahdavi et al., J. of Nucl. Mater. *111, 112*, 355 (1982).

[21]L. Spitzer, *Physics of Fully Ionized Plasmas*, Wiley and Sons Inc., New York (1962).

[23]M.F.A. Harrison, Ref. 9.

[24]The right-hand side Eq.(5) of Ref. 21 has a typographical error. The first bracket should be raised to the 1st power and the second bracket to the 7th power. M.A. Mahdavi, private communication (1987).